Numerical Study Of The Laminer Mixed Convecton In A Ventilated Square Cavity With Baffles

Hussam H. Almsloki*, Ass.Prof. Falah A. Abood, Dr.Emad A. Khazal
***M.Sc. student, E-mail:** hussamhakeem174@yahoo.com
Department of Mechanical Engineering, Engineering College, University of Basrah, Basrah – Iraq

Abstract

Laminar mixed convective flow in a ventilated square cavity with baffle has been studied numerically using finite element method with software package (FlexPDE). The bottom wall is heated with a constant heat flux and the other walls are adiabatic. The flow is assumed to be two-dimensional. The air enters the cavity through an opening at the bottom of the left wall and exits from another opening at the top of the right wall. Laminar regime is considered under steady state condition. In addition, the two horizontal guide baffle, first baffle was attached from the left vertical wall and the other baffle was attached from the right vertical wall with a constant height $H_{b1} = 0.5L$ and length $L_b = 0.25L$ and the third baffle was put in the center with different height $H_{b2} = 0.25L$, $0.5L$ and $0.75L$ and $L_{b1} = 0.4L$. A parametric study was performed presenting the influence of; Reynolds' number ($50 \leq Re \leq 200$), Richardson number ($0.1 \leq Ri \leq 10$) and Prandtl number ($Pr = 0.71$). Results were presented with streamlines, isotherms, Nusselt numbers and average non-dimensional temperature. And the result show the increasing of Nu with increasing Re, Ri and with decreasing the location of the baffle from the bottom wall. A comparison was made between the present work and that obtained by [1] which it reveals good agreement.

Keyword: Mixed Convection, Ventilated, Square Enclosure, Baffle, FEM.

دراسة عددية للحمل المختلط الطباقي في فجوة مربعة مفتوحة مع حواجز

الخلاصة

جريان الحمل المختلط الطباقي داخل فجوة مربعة تحوي فتحات وحواجز تم دراسته عدديا باستخدام طريقه العناصر المحددة بمساعدة الحقيبة المكتبية (FlexPDE). الجدار السفلي يكون مسخن بفيض حراري ثابت والجدران الاخرى تكون معزولة. يفرض الجريان بانه ذو بعدين. الهواء يدخل الى الفجوة من خلال الفتحة في اسفل الجدار الايسر ويخرج من الفتحة الاخرى في اعلى الجدار الايمن. النظام الطباقي يعتبر تحت شروط الحالة المستقرة. بالإضافة، الى وجود حاجزين موجهين بطريقة افقية، الحاجز الاول يتصل بالجدار العمودي الايسر والاخر يتصل بالجدار العمودي الايمن ويكون ارتفاعهما $0.5L$ وطولهما $0.25L$ مع وجود حاجز ثالث ويكون في عدة ارتفاعات وهذه الارتفاعات هي $0.25L$, $0.5L$, $0.75L$ وطوله $0.4L$. في هذه الدراسة تم تمثيل النتائج باستخدام تأثير الثوابت رقم رينولدز يتراوح ($50 \leq Re \leq 200$)، رقم ريكاردسون ($0.1 \leq Ri \leq 10$) ورقم برانتل ($Pr = 0.71$). النتائج قدمت على شكل خطوط الجريان وخطوط ثابتة درجة الحرارة وعدد نسلت مع زيادة عدد ريكاردسون وعدد رينولدز ومع تناقص موقع الحاجز بالنسبة للجدار السفلي المسخن. المقارنة تمت بين العمل الحالي والنتائج التي حصل عليها رحمن [1] والتي اظهرت توافق جيد جدا.

1. Introduction

Heat transfer by mixed convection using the baffle was the subject of many theoretical and experimental studies because of the importance in engineering applications such as nuclear, solar, bio-medical and electronic industry that employ mixed convection. Baffles are used widely in fuel tanks, crankcase, mufflers, radiators and intake system of vehicles because of its unique advantages like changing the fluid flow direction, increasing the retaining time, providing additional surface area for heat transfer, some electronic circuit boards, internally cooled turbine blades, in silencer pipe etc… [2]**.** Natural convection has a limitation in the effective cooling and because of the need for effective cooling methods in the electronic industry. Combined forced and free convection has gained popularity over the years and would continue to do so with the size of all electronic devices shrinking drastically and so now a day. Thus, its study is of paramount importance and today the focus is more on different techniques for enhancing heat transfer in mixed convective flow**.**

Numerical study of opposing mixed convection in a vented enclosure using a finite element method has been performed by [1] The significant parameters are Grashof number, Richardson number and Reynolds number by which different fluid and heat transfer characteristics inside the cavity were obtained. Results show that the enhancement of heat transfer process with increasing of Ri due to dominate of free convection. In [3] carried out a numerical analysis to study the performance of mixed convection in a rectangular enclosure. Four different placement configurations of the inlet and outlet openings were considered with a constant flux heat source on the vertical surface. The results indicated that the average Nusselt number and the dimensionless surface temperature on the heat source strongly depended on the positioning of the inlet and outlet openings. In [4] investigated numerically a steady buoyancy-driven flow of air in a partially open square cavity with internal heat source. The top and bottom walls are adiabatic, and the vertical walls are isothermal. Rayleigh numbers range from 400 to 2000. The results showed that when the flow was controlled mainly by the heat source there are a large secondary circulations inside the cavity and the isotherms exhibited parabolic behavior, causing an increase in the values of Nusselt number. In [5] investigated numerically the mixed convection in a rectangular partitioned cavity equipped with two heated partitions at a constant temperature. The right vertical wall was featured by two openings for entrance of cooled air along the horizontal direction, while the lower wall has a single outlet along the vertical axis. They assumed that the left vertical wall is isothermal at temperature T_C, while the other walls were cooled to a temperature $T_F < T_C$. The results show that of the range Reynolds number ($10 \leq Re \leq 100$), the heat transfer process was increased with increasing Re and further increment in heat transfer will occur with increasing the partitions size. In [6] studied numerically of laminar mixed convective cooling in a ventilated cavity utilizing a guide baffle. The bottom wall was heated with constant heat flux. The horizontal guide baffle with different locations was attached from the left vertical wall. A parametric study was performed presenting the influence of Reynolds number ($50 \leq Re \leq 500$), Richardson number ($0.01 \leq Ri \leq 10$)**.** They observed that, if the baffle location from the heat flux part decreased it assists the forced convection mode and oppose the natural convection mode, so for Ri = 0.01 to 1, the natural convection was very small with respect to forced convection and for high values of Ri and lower values of Re the existence of baffle decreased the heat transfer rate. In [7] presented numerical study of finite difference based two-dimensional of steady laminar natural convection inside the open square enclosure with protrusions. All the external peripheral walls were considered as hot and the interior cross walls were assumed as cold. The heat transfer process for natural convection was enhanced further through the Rayleigh number by varying Ra as 10^3, 10^4 and 10^5. The results showed that the introduction of cold baffle intensifies the heat transfer inside the enclosure irrespective of its position and length. Also, the simultaneous placing of baffle on both sides reduces the variations of heat transfer between the left face and right face of the vertical partition on the top wall of enclosure. In [8] investigated numerically the periodic unsteady natural convection flow and heat transfer in a square enclosure containing a concentric circular cylinder. The temperature of the inner cylinder was high, while the temperature of the enclosure was low. The two-dimensional natural convection was simulated with high accuracy method. The Rayleigh number was ranged $10^3 \leq Ra \leq 10^6$, the temperature pulsating period ranged from 0.01 – 100 and the temperature pulsating amplitudes 0.5, 1 and 1.5. They founded that the heat transfer of the time-periodic unsteady natural convection is enhanced comparing with steady state case generally. With increasing of Rayleigh number and temperature pulsating amplitude, the heat transfer rate is increased. Maximum enhancement of heat transfer was observed when $Ra = 10^5$ and 10^6.

2. Model Description

The model considered here is a square ventilated cavity with baffle (two baffle are attacked with left and right vertical wall and the third baffle is moved at different location in the cavity H_{b2} = 0.25, 0.5, 0.75). The bottom wall is subjected to a constant heat flux (q″) as shown in Fig. 1. While the other walls are taken as adiabatic except the opening position. The entrance of the cold fluid occurs through the inflow opening with uniform velocity (u_{in}) and ambient temperature (T_{in}). The characteristic length (L), the height (H) of the cavity are constant and the length of the two fixed baffles equals L_b = 0.25L and the length of third baffle L_{b1} = 0.4L. The thickness of all baffle (t = 0.04L). The inflow opening located on the lower left vertical wall and the outflow opening is located on the top right vertical wall. For simplicity, the height of the two openings for all geometric models is kept the same size and equal to w = 0.1H.

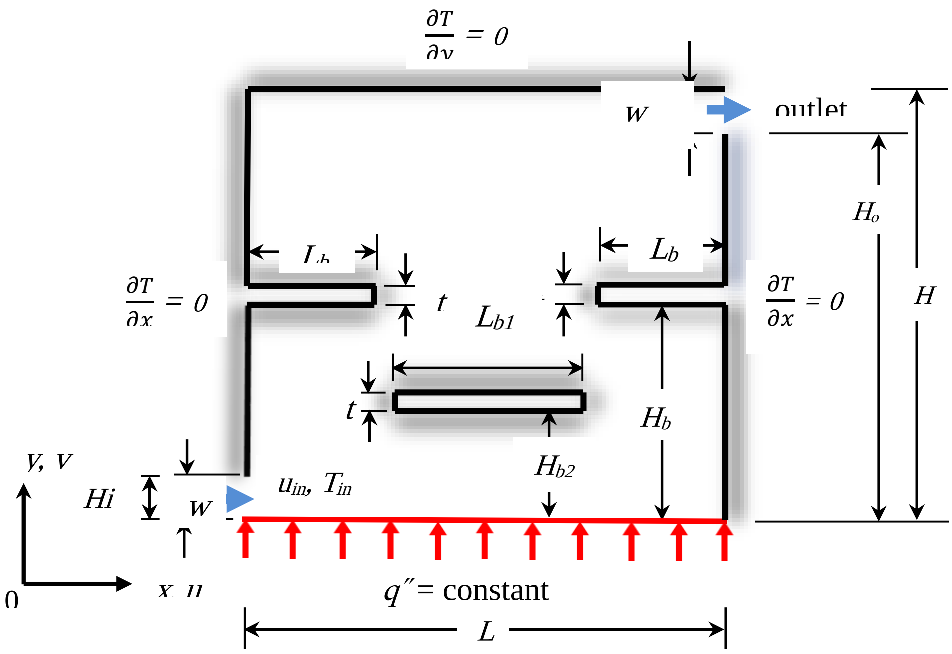

Fig. 1 Schematic diagram of the problem.

3. Mathematical Formulation

Mixed convection is governed by the differential equations expressing conservation of mass, momentum and energy. The viscous dissipation term in the energy equation is neglected. The Boussinesq approximation is raised for the fluid properties to relative density changes to temperature changes. The governing equations, for the present study are based on the following assumptions; the flow is two-dimensional, incompressible, laminar and steady state, the fluid is assumed to be Newtonian, the fluid is air with constant physical properties but obeys the Boussinesq approximation according to which the compressibility effect everywhere is neglected except for the buoyancy force term and the viscous dissipation term in the energy equation while internal heat generation and radiation heat transfer is negligible.

Under the above assumption the governing equations can be written in non-dimensional form as follows: [9]

- Continuity equation:

$$\frac{\partial U}{\partial X} + \frac{\partial V}{\partial Y} = 0 \tag{1}$$

- Momentum equation:

$$U\,\frac{\partial U}{\partial X} + V\frac{\partial U}{\partial Y} = -\frac{\partial P^*}{\partial X} + \frac{1}{Re}\left(\frac{\partial^2 U}{\partial X^2} + \frac{\partial^2 U}{\partial Y^2}\right) \tag{2}$$

And

$$U\,\frac{\partial V}{\partial X} + V\frac{\partial V}{\partial Y} = -\,\frac{\partial P^*}{\partial Y} + \frac{1}{Re}\left(\frac{\partial^2 V}{\partial X^2} + \frac{\partial^2 V}{\partial Y^2}\right) + \frac{Gr}{Re^2}\theta \tag{3}$$

- Energy equation:

$$U\,\frac{\partial \theta}{\partial X} + V\frac{\partial \theta}{\partial Y} = \frac{1}{Re\,Pr}\left(\frac{\partial^2 \theta}{\partial X^2} + \frac{\partial^2 \theta}{\partial Y^2}\right) \tag{4}$$

- Stream function :

$$\frac{\partial^2 \psi}{\partial X^2} + \frac{\partial^2 \psi}{\partial Y^2} = \frac{\partial U}{\partial Y} - \frac{\partial V}{\partial X} \tag{5}$$

The dimensionless variables are defined as:

$$X = \frac{x}{L},\quad Y = \frac{y}{H},\quad N = \frac{n}{L},\quad U = \frac{u}{u_{in}},\quad V = \frac{v}{u_{in}}$$

$$\theta = \frac{T - T_{in}}{T_h - T_{in}} = \frac{k(T - T_{in})}{q''L},\qquad P^* = \frac{p}{\rho u_{in}^2},\quad \psi = \frac{\varphi}{L\,u_{in}}$$

Where X and Y are dimensionless coordinates varying along horizontal and vertical directions respectively, U and V are dimensionless velocity components in the X and Y directions respectively, θ is the dimensionless temperature and $P*$ is the dimensionless pressure. The non-dimensional numbers seen in the above Gr, Re, Ri and Pr are the Grashof number, Reynolds number, Richardson number and Prandtl number respectively [10]:

$$Gr = \frac{g\beta L^3 q}{k v^2},\quad Re = \frac{u_{in}L}{v},\qquad Ri = \frac{Gr}{Re^2},\quad Pr = \frac{v}{\alpha}$$

3.1 Boundary Conditions

Based on the dimensionless parameters the non-dimensional boundary conditions are:

1- At the inlet: $U = 1, V = 0 \;\&\; \theta = 0$
2- At the exit: $\frac{\partial U}{\partial X} = 0, V = 0, P^* = 0 \;\&\; \frac{\partial \theta}{\partial X} = 0$
3- Wall thermal conditions: (constant heat flux in the bottom wall): $\frac{\partial \theta}{\partial Y} = -1$
4- $\frac{\partial \theta}{\partial N} = 0$ (adiabatic other walls of the cavity and the baffles).
5- No slip condition on the solid surface; $U = 0, V = 0$

3.2 Heat Transfer Parameter

The local Nusselt number along the bottom wall is defined as:

$$Nu_L = -\frac{\partial \theta}{\partial Y} \tag{6}$$

The average Nusselt number at the bottom wall is :

$$\overline{Nu} = \frac{1}{L}\int_0^L Nu_L\,dx \tag{7}$$

where (L) is the length of the heated bottom wall.

The bulk average temperature is defined as:

$$\theta_{av} = \frac{\int \theta d\bar{V}}{\bar{V}} \quad (8)$$

Where: $\bar{V}$ is the volume of occupying fluid in the cavity, which should be minimized.

4. Computational Procedure

In the present study, a finite element software package FlexPDE is applied in the solution of the nonlinear system of equations (1) to (4) Fig. 2 show that [11]. Hence, the continuity equation (1) is used to check the error of the solution throughout the grids of domain. The penalty finite element method are applied to overcome the linkage between velocity and pressure in the momentum equations using the continuity equation [12]. The following equation is the program used in the solution:

$$\nabla^2 P = \lambda \left(\frac{\partial U}{\partial X} + \frac{\partial V}{\partial Y} \right) \quad (9)$$

Where: λ is a setting parameter. There is an automatic satisfaction of the continuity equation for large value of penalty parameter λ [11]. 10^5 is the typical value of λ that yields consistent solution while 10^{-3} is the relative error limit which is employed in this study.

The system of equations (2), (3), (4) and (9) are solved by using any method in finite element such as Galerkin finite element method at which the code FlexPDE has been depended in the solution [13, 11]. Expanding the velocity components *(U, V)*, *(P)* and temperature *(θ)* using basis set $\{\Phi_k\}_{k=1}^{n}$ as,

$$U \approx \sum_{k=1}^{n} U_K \, \Phi_K(X,Y)$$
$$V \approx \sum_{k=1}^{n} V_K \, \Phi_K(X,Y)$$
$$p \approx \sum_{k=1}^{n} p_K \, \Phi_K(X,Y)$$
$$\theta \approx \sum_{k=1}^{n} \theta_K \, \Phi_K(X,Y) \quad (10)$$

Where: $\Phi_k(X,Y)$ The shape function which is exemplified in the next analysis the Galerkin finite element method yields the following nonlinear residual equations for Eqs. (2), (3), (4) and (9) respectively, at nodes of internal domain (Ω):

$$R_{i(x,y)}^{(1)} = \sum_{k=1}^{n} U_K \int_\Omega \left[\left(\sum_{k=1}^{n} U_K \Phi_K(X,Y) \right) \frac{\partial \Phi_K}{\partial X} + \left(\sum_{k=1}^{n} V_K \Phi_K(X,Y) \right) \frac{\partial \Phi_K}{\partial Y} \right] \Phi_i \, dX\, dY + \lambda \left[\sum_{k=1}^{n} U_K \int_\Omega \frac{\partial \Phi_i}{\partial X} \frac{\partial \Phi_K}{\partial X} dX\, dY + \sum_{k=1}^{n} V_K \int_\Omega \frac{\partial \Phi_i}{\partial X} \frac{\partial \Phi_K}{\partial Y} dX\, dY \right] + \frac{1}{Re} \sum_{k=1}^{n} U_K \int_\Omega \left[\frac{\partial \Phi_i}{\partial X} \frac{\partial \Phi_K}{\partial X} + \frac{\partial \Phi_i}{\partial Y} \frac{\partial \Phi_K}{\partial Y} \right] dX\, dY \quad (11)$$

$$R_{i(x,y)}^{(2)} = \sum_{k=1}^{n} V_K \int_\Omega \left[\left(\sum_{k=1}^{n} U_K \Phi_K(X,Y) \right) \frac{\partial \Phi_K}{\partial X} + \left(\sum_{k=1}^{n} V_K \Phi_K(X,Y) \right) \frac{\partial \Phi_K}{\partial Y} \right] \Phi_i \, dX\, dY + \lambda \left[\sum_{k=1}^{n} U_K \int_\Omega \frac{\partial \Phi_i}{\partial Y} \frac{\partial \Phi_K}{\partial X} dX\, dY + \sum_{k=1}^{n} V_K \int_\Omega \frac{\partial \Phi_i}{\partial Y} \frac{\partial \Phi_K}{\partial Y} dX\, dY \right] + \frac{1}{Re} \sum_{k=1}^{n} V_K \int_\Omega \left[\frac{\partial \Phi_i}{\partial X} \frac{\partial \Phi_K}{\partial X} + \frac{\partial \Phi_i}{\partial Y} \frac{\partial \Phi_K}{\partial Y} \right] dX\, dY - Ri \int_\Omega \left(\sum_{k=1}^{n} \theta_K \Phi_K(X,Y) \right) \Phi_i \, dX\, dY \quad (12)$$

$$R_{i(x,y)}^{(3)} = \sum_{k=1}^{n} \theta_K \int_\Omega \left[\left(\sum_{k=1}^{n} U_K \Phi_K(X,Y) \right) \frac{\partial \Phi_K}{\partial X} + \left(\sum_{k=1}^{n} V_K \Phi_K(X,Y) \right) \frac{\partial \Phi_K}{\partial Y} \right] \Phi_i \, dX\, dY + \frac{1}{Re\, Pr} \sum_{k=1}^{n} \theta_K \int_\Omega \left[\frac{\partial \Phi_i}{\partial X} \frac{\partial \Phi_K}{\partial X} + \frac{\partial \Phi_i}{\partial Y} \frac{\partial \Phi_K}{\partial Y} \right] dX\, dY \quad (13)$$

$$R_{i(x,y)}^{(4)} = \sum_{k=1}^{n} p_k \int_\Omega \left[\frac{\partial \Phi_i}{\partial X} \frac{\partial \Phi_K}{\partial X} + \frac{\partial \Phi_i}{\partial Y} \frac{\partial \Phi_K}{\partial Y} \right] dX\, dY - \lambda \left[\sum_{k=1}^{n} V_k \left(\int_\Omega \frac{\partial \Phi_k}{\partial X} \right) \Phi_i dX dY + \sum_{k=1}^{n} V_k \left(\int_\Omega \frac{\partial \Phi_k}{\partial Y} \right) \Phi_i dX dY \right] \quad (14)$$

The usual of non-linear algebraic equations (11), (12), (13) and (14) are solved using the code FlexPDE.

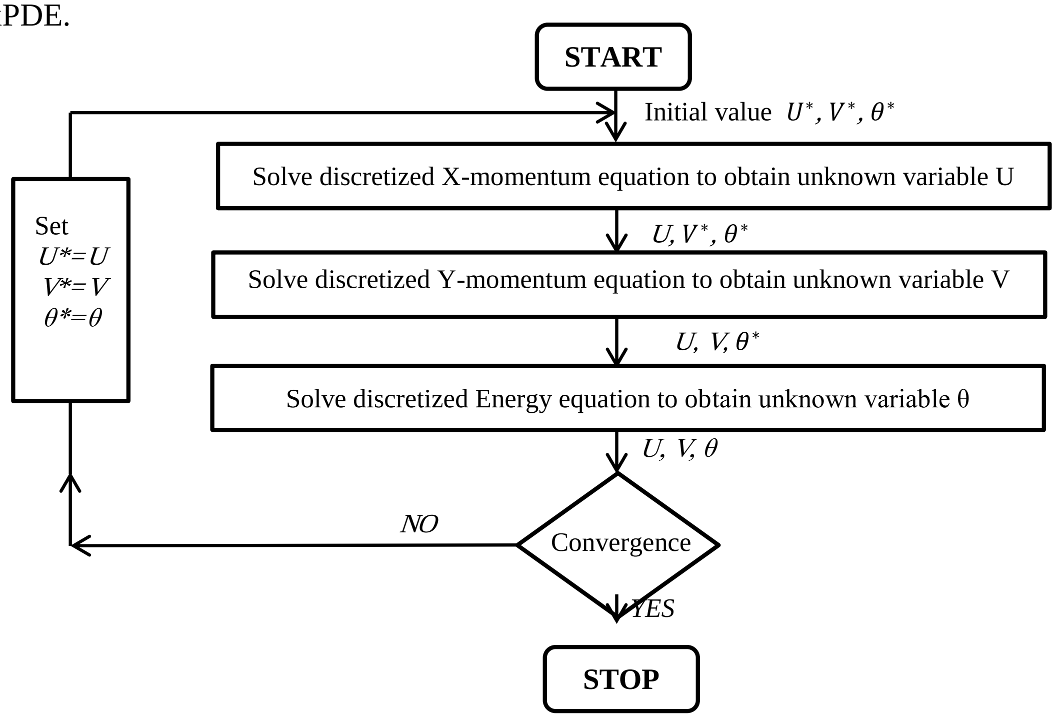

Fig. 2: Flowchart of computer program numerical solution by using the code FlexPDE.

4.1 Grid Refinement Check

The grid dependency is checked together with continuity equation and obtained results showed an exactly validation of the velocity distribution for a grid size obtained by imposing an accuracy of 10^{-3}. This accuracy is compromised value between the result accuracy and the time consumed in each run. The mesh mode for the present numerical computation for *Re* = 100 and Ri =1 is shown in Fig. 3.

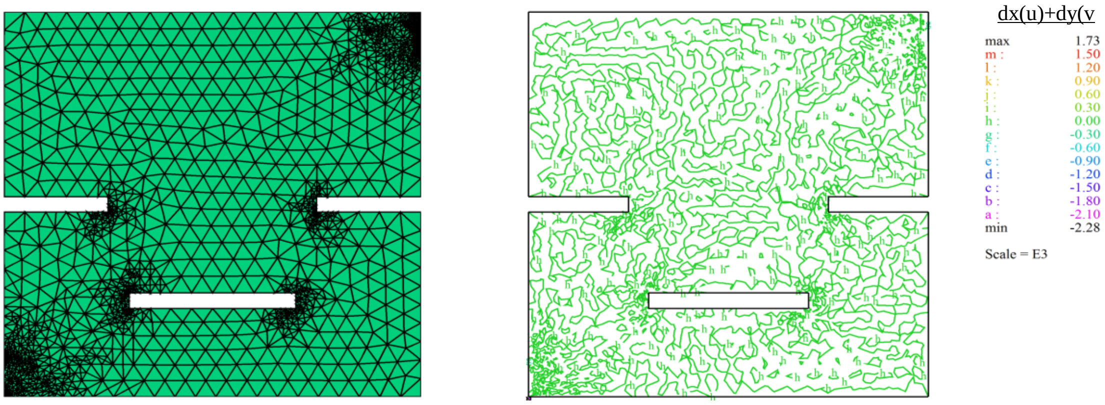

Fig. 3: (a) Grid distribution over the domain. (b) validation of continuity equation.

4.2 Code Validation

A computational model is validated for mixed convection heat transfer by comparing the correlation numerical study of opposing mixed convection in a vented enclosure with uniform heat flux in left wall and the other wall is insulated [1]. For *Hi* = 0.2*L*, *Re* =100 and *Pr* = 0.71*L*. For the same parameters used in Rahaman et al. (2007) and the values of average

Nusselt number ($\overline{Nu}$) and average fluid temperature (θ_{av}) are shown in Table.1 and Table. 2 respectively. Fig. 3 shows the comparison of the thermal fields between the present investigation and Rahaman et al. (2007). The results show a good agreement.

Table 1: Effect of *Ri* on $\overline{Nu}$ for *Hi* = 0.2*L*, *Re* = 100 and *Pr* = 0.71.

Ri	Present work $\overline{Nu}$	(Rahman et al., 2007)[1] $\overline{Nu}$	Error (%)
1	1.820655	1.824	0.18338
10	2.300314	2.295	0.23154

Table 2: Effect of *Ri* on θ_{av} for *Hi* = 0.2*L*, *Re* = 100 and *Pr* = 0.71.

Ri	Present work θ_{av}	(Rahman et al., 2007)[1] θ_{av}	Error (%)
1	0.049308	0.049231	0.15640
10	0.043279	0.042996	0.65351

Isotherms

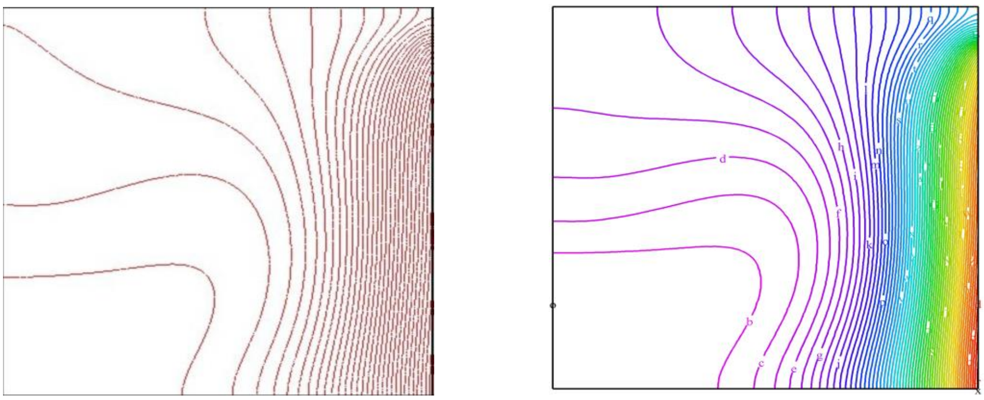

Present work (Rahman et al. (2007))

Fig. 3: Comparison of isotherms for validation at *Re* = 00, *Ri* = 1, *Hi* = 0.2*L* and *Pr* = 0.71.

5. Results and Discussion

5.1 Flow and Thermal Fields Characteristics

In this paper, the mixed convection flow inside a ventilated cavity is numerically investigated. The stream lines and isotherms has been on the left and right respectively as shown in Figs. 4, 5 and 6.

Fig. 4 (on the left) shows the effect of different *Re* on the streamlines for square cavity with baffle when $H_{b1} = 0.5L$, H_{b2}=0.25*L*, $L_b = 0.25L$, L_{b1} = 0.4*L*, *Hi* = 0 and *Ri* = 1. It can be seen at *Re* = 50, the streamlines concentrated at the upper part of the altered baffle and one cellular motion is formed at upper space of the left baffle due to dominance the equivalence natural convection. For *Re* = 100, the maximum value of streamlines density is reduced at the upper part and vice-versa at the baffle space when it is comprised with Re = 50 and the recirculation cell reduces in size. When *Re* is increased to 200, the maximum intensity of stream function is increased and the multi cellular motion is formed near the entrance region due to the blockage effect. The right side of this figure shows the distribution of the isotherms, at low *Re* the isotherms are covered the lower half of the cavity due to the dominance of free convection and the presence of baffle. At large value of Re the thin of the thermal boundary layer is decreased and the thermal lines are concentrated near the heated surface due to dominance the forced convection. **Fig. 5** (on the left) depicts the effect of *Ri* on the streamlines for different baffle location and different baffle length $H_{b1} = 0.5L$, H_{b2} = 0.25L, $L_b = 0.25L$, L_{b1} = 0.4L, *Hi* = 0 and *Re* = 100. When *Ri* = 0.1, one cell is formed above the left baffle. At *Ri* = 1, the stream lines shows the same trend of Ri = 0.1, but the maximum intensity of stream lines are a little decrease in value. With increasing *Ri* = 10, the stream lines density is increased near the heated surface and maximum stream function value is increased. A cellular motion is formed at the upper part of the left baffle due to the effect of the secondary flow and the blockage effect. It can be observed from the left side of this figure that at low *Ri*, the isotherm are equivalent in the upper left part of the cavity, and with increasing of *Ri* the isotherms lines are concentrated near the heated surface and the thickness of the thermal boundary layer is increased due to dominance of free convection. **Fig. 6** (on the left)) illustrates the effect of different location of constant baffle (H_{b2} = 0.25L, 0.5L and 0.75L) on the streamlines counter in the square cavity when $H_{b1} = 0.5L$, $L_b = 0.25L$, L_{b1} = 0.4L and *Hi* = 0 for *Re* = 100, *Ri* = 1. When H_b = 0.25L, the stream lines are concentrated in the middle cavity space and one cell is formed at the upper of the left baffle. When H_{b2} = 0.5L, the recirculating cells are confined at the upper and lower left side of the cavity due to resistance to flow. When H_{b2} = 0.75L, the maximum intensity is more than at H_{b2} = 0.25L, 0.5L and a single recirculation cell is formed because of reducing the resistance to the flow and this lead to enhancement the heat transfer process. Figure shows an increases of stream lines intensity with increasing H_{b2} due to decreasing the flow resistance, and this decrement of the resistance because low blockage effect. For the isotherms (on the right), the temperature is equal in all elevation as appear in the upper space of the left part of the cavity. The growth of the thermal boundary layer is increased with increasing of H_{b2} due to the reducing of flow resistance.

5.2 Heat Transfer Characteristics

Fig. 7 (on the left) clears the variation of local Nusselt number along the heated surface at *Re* = 100 for different Ri and different height of the constant baffle H_{b2}= 0.25, 0.5 0.75. **Fig. 7a** to **Fig. 7c** shows the variation of local Nusselt number (Nu_L). It can be noticed that the local Nusselt number is decreased gradually along the heated bottom wall toward the right corner of the cavity because a large temperature difference, as well as the thickness of the thermal boundary layer is a little. The heat transfer rate is increased with increasing of *Ri* due to the effect of the free convection. At *Ri* = 0.1, 1 the rate of heat transfer almost equal inside the enclosure because the dominance of forced convection. It can be seen that the Nu_L is reduced with increase of H_{b2} and there is a small effect of H_{b2} on the heat transfer process**. Fig. 8** (on the right) shows the variation of the average Nusselt number with Ri for different Re. **Fig. 8a** illustrates the variation of $\overline{Nu}$ for H_{b2} = 0.25L, it can be seen from this figure that for all values of *Re* a gradually increasing of average Nusselt number with increasing of *Ri*. For the range of *Ri* from 0.1 – 1, it can be shows a slightly increasing of average Nusselt number due to the dominance of the forced convection. When *Re* = 200 the average Nusselt number is increased because of decreasing in the growth of the boundary layer near the heated surface. **Fig. 8b** predicts the average Nusselt number with *Ri* for different value of *Re* at H_{b2} = 0.5. For low *Re*, figure shows a reducing of the $\overline{Nu}$ value when it is comprised with Fig. 8a due to the reducing to the resistance of the flow. **Fig. 8c** shows the variation of average Nusselt number for H_{b2} = 0.75L. The trend of $\overline{Nu}$ curves is the same as that in Fig. 8b. And the values of $\overline{Nu}$ are higher than that in Fig. 8b, this is due to decrease in resistance to flow.

5.3 Mean Bulk Temperature (θ_{av})

Fig. 9 represents the variation of mean bulk temperature with *Ri* for different value of *Re*. For H_{b2} = 0.25*L* as shown in **Fig. 9a**, it can be seen that the mean bulk temperature is increased with decreasing of *Re*, and is decreased with increasing of *Ri* due to decreasing of the flow rate and thickness of the thermal boundary layer. **Fig. 9b** and **Fig. 9c** show the variation of mean bulk temperature with *Ri* for H_{b2} = 0.5*L*, 0.75*L* respectively. This figure show a slight increase of θ_{av} with increasing of the baffle height H_{b2}. This is because of increasing the resistance to flow with low H_{b2} and leading to the growth the thermal boundary layer.

6. Conclusions

A numerical investigation on mixed convection in a square ventilated cavity with different location of baffle was carried out by a finite element method using the software package (FlexPDE). The present study reveals the following conclusion:

1- When increases the baffle location the average Nusselt number decrease due to decrease the resistance to the flow.
2- The thermal performance in terms of both average Nusselt numbers and the average fluid temperature are affected by Ri. They are increases with increasing Ri for all location of baffle.
3- If the baffle location H_b decreases it assists the forced convection mode and oppose the natural convection mode.
4- The exit port location do not has significant effects on the heat transfer process.

References

[1] Rahman, M.M. Alim, Mamun M.A., Chowdhury M.A.H., M.K. and Islam, A.K.M. S., "Numerical Study of Opposing Mixed Convection in a Vented Enclosure", ARPN Journal of Engineering and Applied Sciences, Vol. 2, No. 2, pp. 25 – 36, (2007).

[2] Asif M. R., Hossain M. S. and Hossain K. A., "Heat Transfer in a Rectangular Enclosure with Baffles", ARPN Journal of Engineering and Applied Sciences, Vol. 6, No. 4, pp. 29 – 41, (2011).

[3] Saha, S., Mamun, Hossain A.H., M.Z. and Sadrul Islam, A.K.M.,"Mixed Convection in an Enclosure with Different Inlet and Exit Configurations", Journal of Applied Fluid Mechanics, Vol.1, No.1, pp. 78 – 93, (2008).

[4] Fontana E., A. da Silva and Mariani V. C., "Natural Convection in a Partially Open Square Cavity with Internal Heat Source: An Analysis of the Opening Mass Flow", International Journal of Heat and Mass Transfer, Vol. 54, pp. 1369–1386, (2011).

[5] Mahrouche O., Najam M., El Alami M. and Faraji M., "Mixed Convection Investigation in an Opened Partitioned Heated Cavity", Tech Science Press, Vol. 9, No. 3, pp. 235 – 250, (2013).

[6] El-Maghlany Wael M., Mohamed A. T., Ahmed M. Hanafy, Akram Zeid, "Studied Numerically of Laminar Mixed Convective Cooling in a Ventilated Cavity Utilizing a Guide Baffle", CFD Computational Fluid Dynamic Letters, Vol. 5, No. 4, pp. 197 – 207, (2013).

[7] Kalidasan K., Velkennedy R. and Kanna P. R., "Buoyancy Enhanced Natural Convection Inside the Ventilated Square Enclosure with a Partition and an Overhanging Transverse

Baffle", International Communications in Heat and Mass Transfer, Vol. 56, pp. 121 – 132, (2014).

[8] Huang Z., Zhang W. and Xi G., "Natural Convection in Square Enclosure Induced by Inner Circular Cylinder with Time-Periodic Pulsating Temperature", International Journal of Heat and Mass Transfer, Vol. 82, PP. 16–25, (2015).

[9] Incropera F.P., Dewitt D.P., Bergman T.L. and Lavine A.S., "Fundamentals of Heat and Mass Transfer", Wiley, 6th edition, (2007).

[10] Rahman, M.M., Alim M.A., Saha S. and Chowdhury M.K.,"Effect of The Presence of a Heat Conducting Horizontal Square Block on Mixed Convection Inside a Vented Square Cavity", Nonlinear Analysis: Modelling and Control, Vol. 14, No. 4, p.531–548, 2009.

[11] Backstrom Gunnar, "Fields of Physics by Finite Element Analysis Using FlexPDE," by GB Publishing and Gunnar Backstrom Malmo, Sweden, 2005.

[12] Langtangen H. P., Mardal K. A. and Winther R., "Numerical Methods for Incompressible Viscous Flow", Advances in Water Resources, Vol. 25, pp. 1125 – 1146, (2002).

[13] Tanmay Basak , Roy S., Pawan Kumar Sharma, and Pop I., "Analysis of Mixed Convection Flows Within A Square Cavity with Uniform and Non-uniform Heating of Bottom Wall", International Journal of Thermal Sciences, Vol. 48, p. 891–912, 2009.

Nomenclature

Gr : Grashof number
g : gravitational acceleration (ms^{-2})
L : length of the cavity (m)
L_b :length of baffle (m)
H :high of the cavity (m)
Hi : inlet port location (m)
H_o : outlet port location (m)
H_b :height of baffle (m)
t : thickness of baffle (m)
n : normal direction on a plane (m)
N : number of nodes in the element
$\overline{Nu}$: average Nusselt number
Nu_L : local Nusselt number
P : pressure (Nm^{-2})
P^* : non-dimensional pressure
Pr : Prandtl number
q'': *heat flux* (W/m^2)
R: correlation coefficient
Re : Reynolds number
Ri : Richardson number
T : temperature (K)
T_h : hot temperature (K)
Tin : *inlet temperature* (K)
u, v : velocity components (ms^{-1})
U, V : non-dimensional velocity components
W : height of the inflow and outflow openings
x, y : Cartesian coordinates (m)
X, Y : non-dimensional Cartesian coordinates

Greek symbols:

α:thermal diffusivity, $k/\rho C_p$ (m^{2}s^{-1})
β: thermal expansion coefficient (K^{-1})
λ: penalty parameter
θ: non-dimensional temperature
θ_{av} : average non-dimensional temperature
ν : kinematic viscosity of the fluid (m^{2}s^{-1})
ρ: density of the fluid (kgm^{-3})
Φ: basis functions
φ : stream function
Ψ : non-dimensional stream function

Subscripts:

i : residual number
k : node number

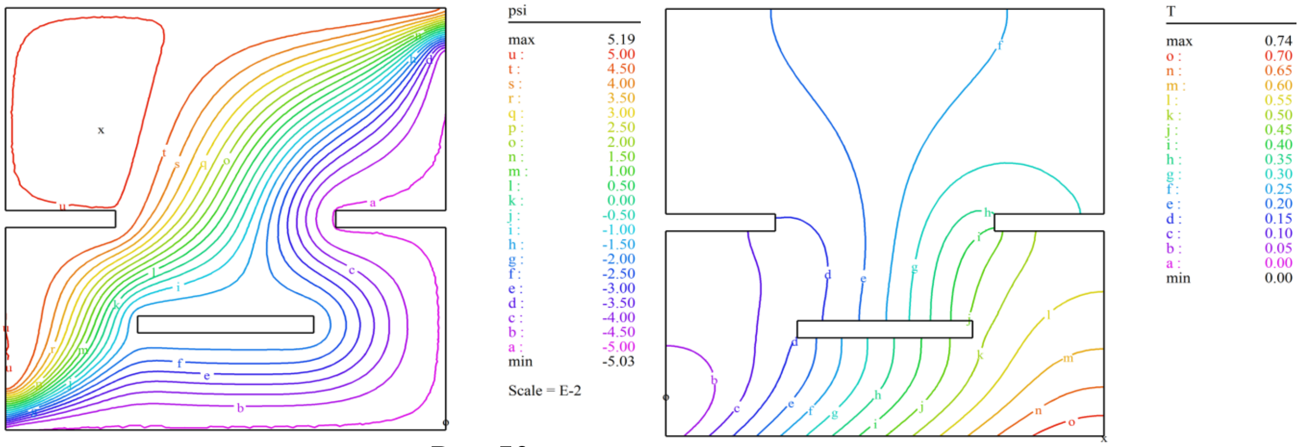

***Re* = 50**

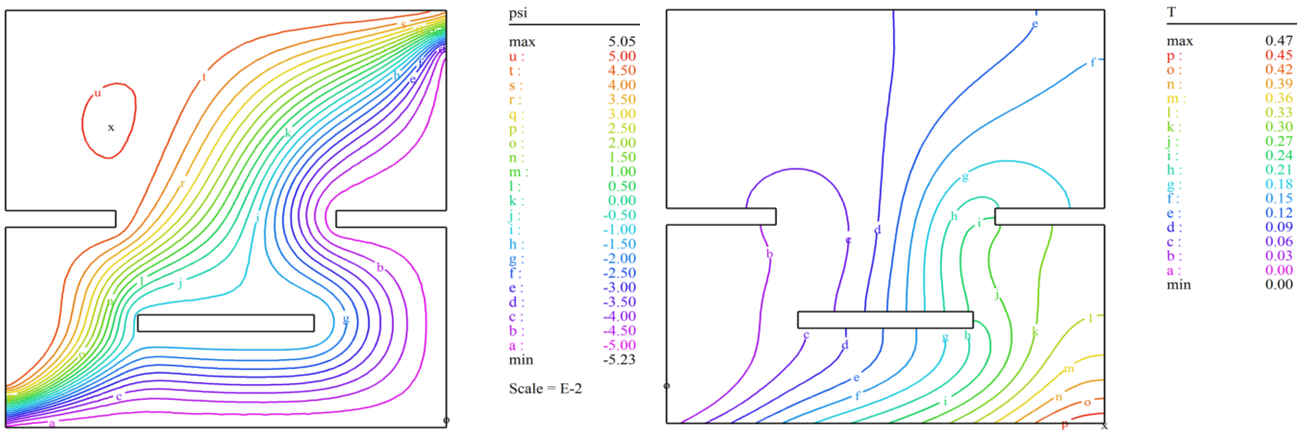

***Re* = 100**

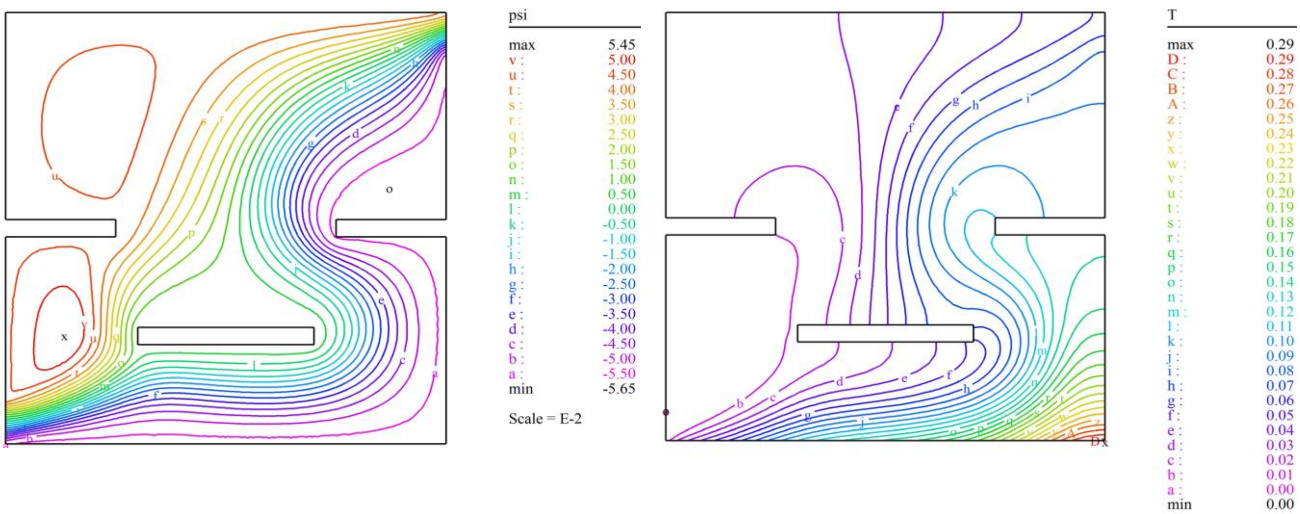

***Re* = 200**

Fig. 4 Streamlines (left) and isotherms (right) contours at *Ri*=1, H_{b1} = *0.5L*,

***H_{b2}*=0.25, *L_b* = *0.25L*, *L_{b1}* = 0.4*L*, and *Hi* = 0.**

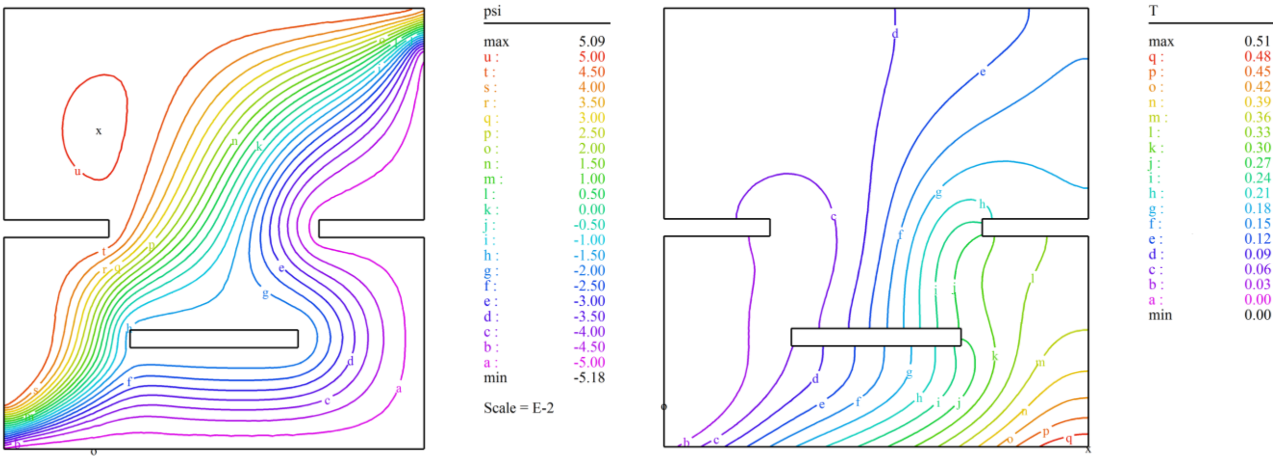

***Ri* = 0.1**

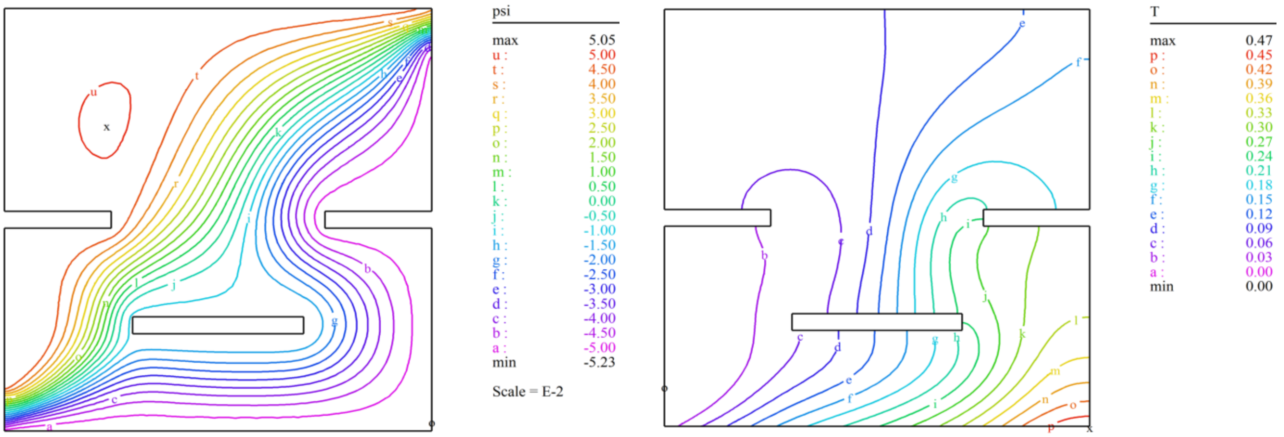

***Ri* = 1**

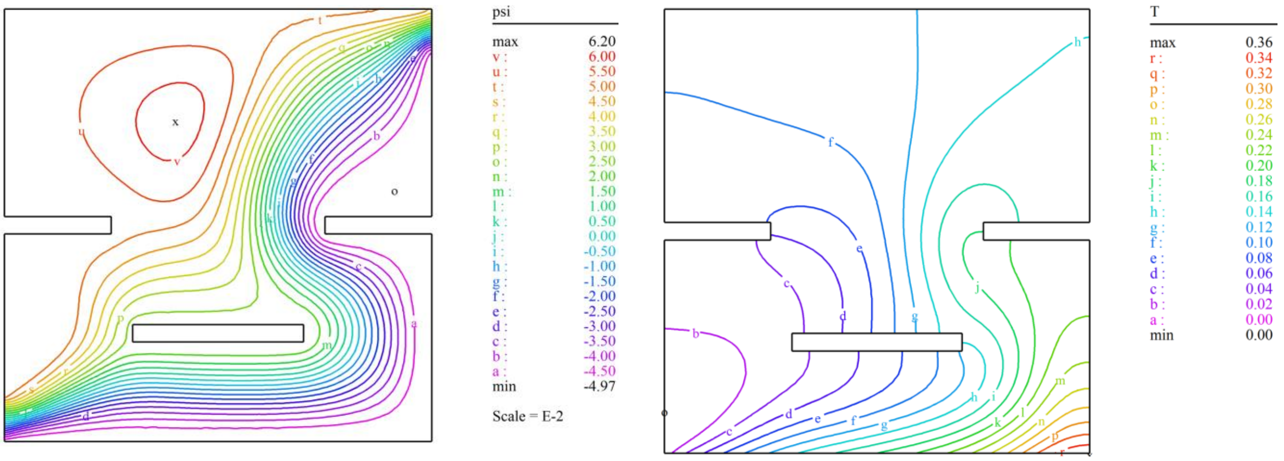

***Ri* = 10**

Fig. 5 Streamlines (left) and isotherms (right) contours at *Re* = 100,

H_{b1}= 0.5L, H_{b2}=0.25, L_b = 0.25L, L_{b1} = 0.4L*, and *Hi = 0.

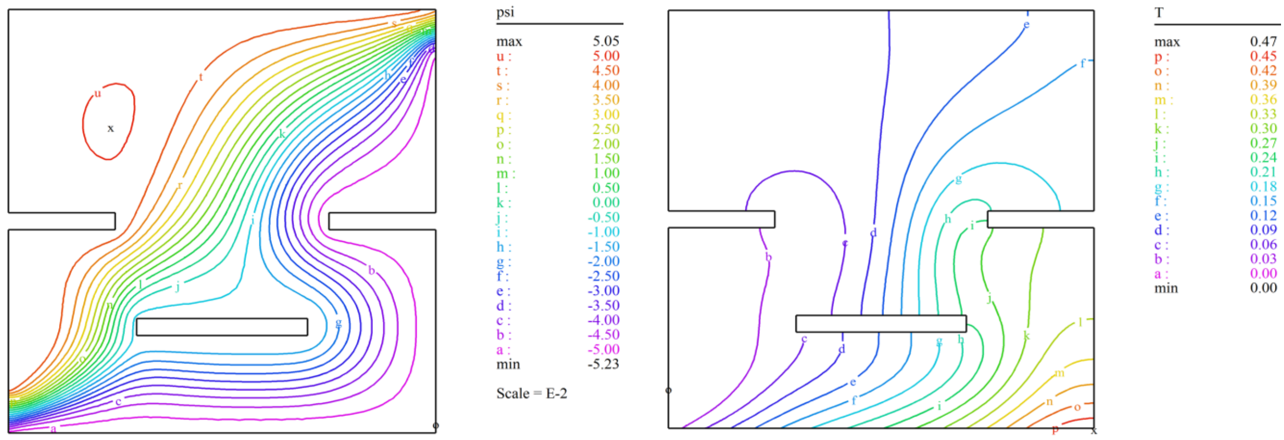

H_{b2}* = 0.25*L

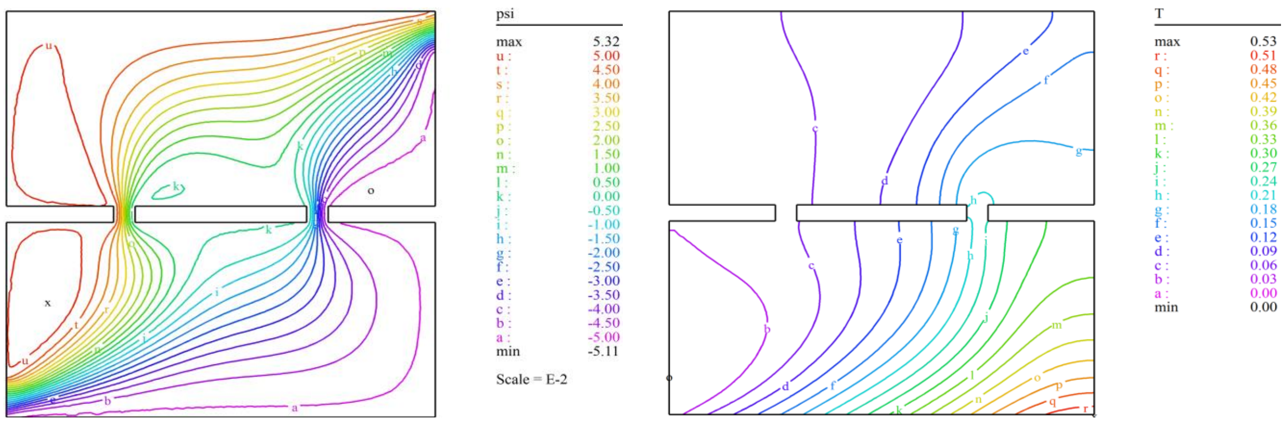

H_{b2}* = 0.5*L

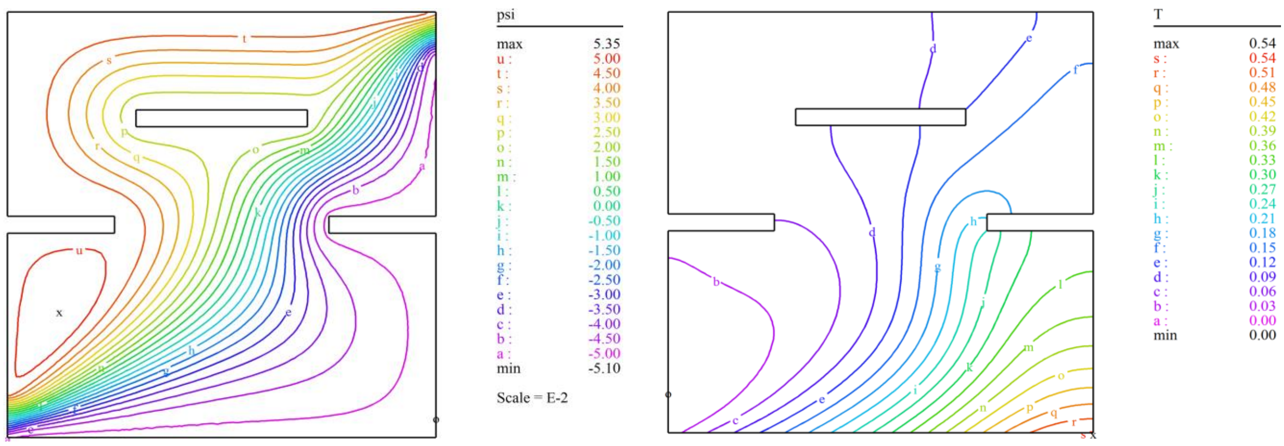

H_{b2}* = 0.75*L

Fig. 6 Streamlines (left) and isotherms (right) contours at *Re* = 100, *Ri* = 1, *H_{b1} = 0.5L*, *L_b = 0.25L*, *L_{b1}*=0.4*L*, and *Hi*=0.

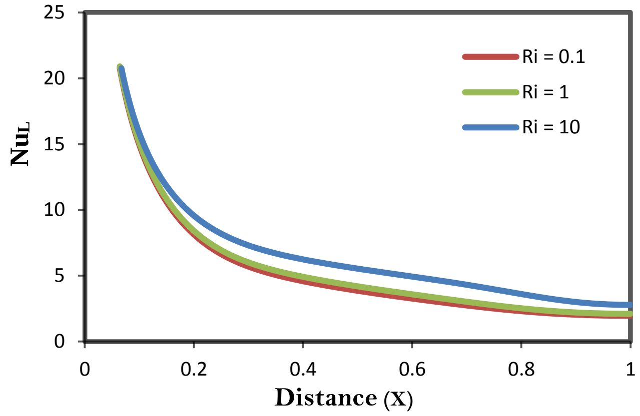

(a)

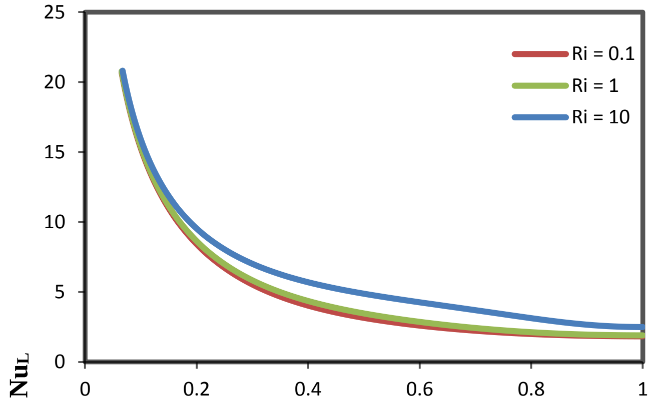

(b)

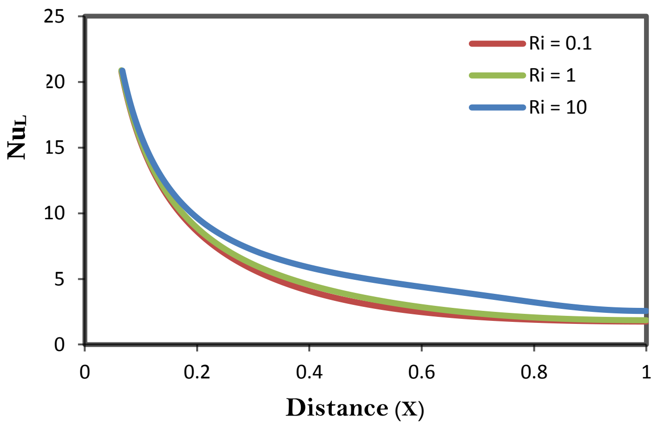

(c)

Fig. 7 Variation of local Nusselt number along the heated surface at Re=100: (a)H_{b2}=0.25L , (b) H_{b2}=0.5L , (c) H_{b2}=0.75L.

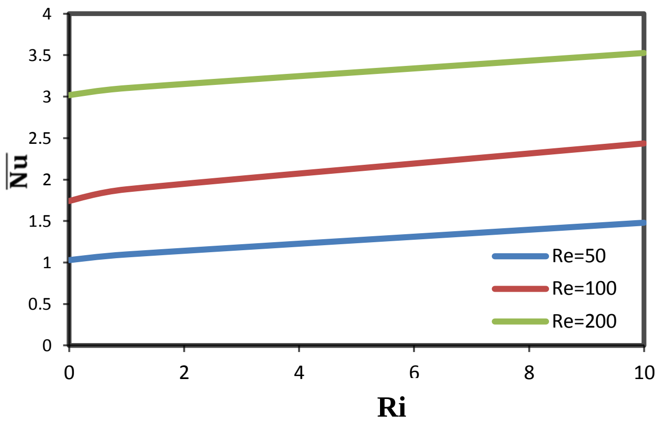

(a)

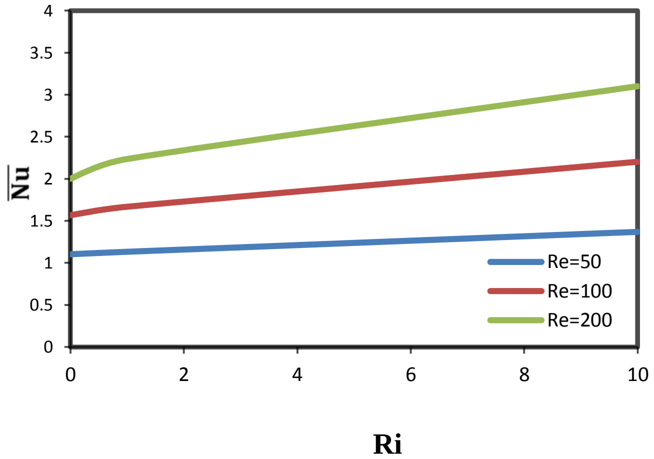

(b)

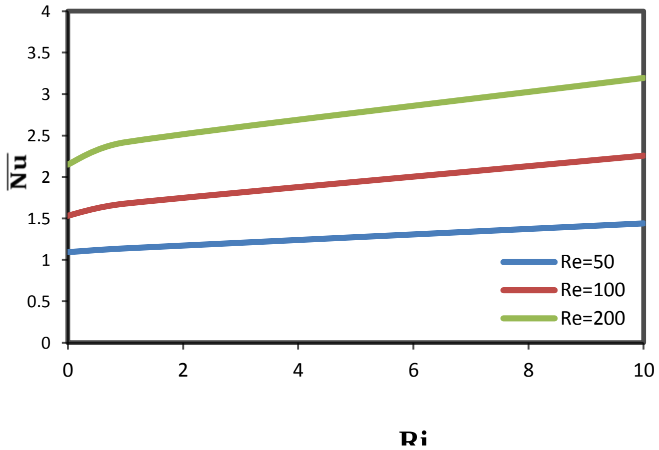

Fig. 8 Variation of average Nusselt number with Ri: (a) H_{b2}=0.25L , (b) H_{b2}=0.5L , (c) H_{b2}=0.75L.

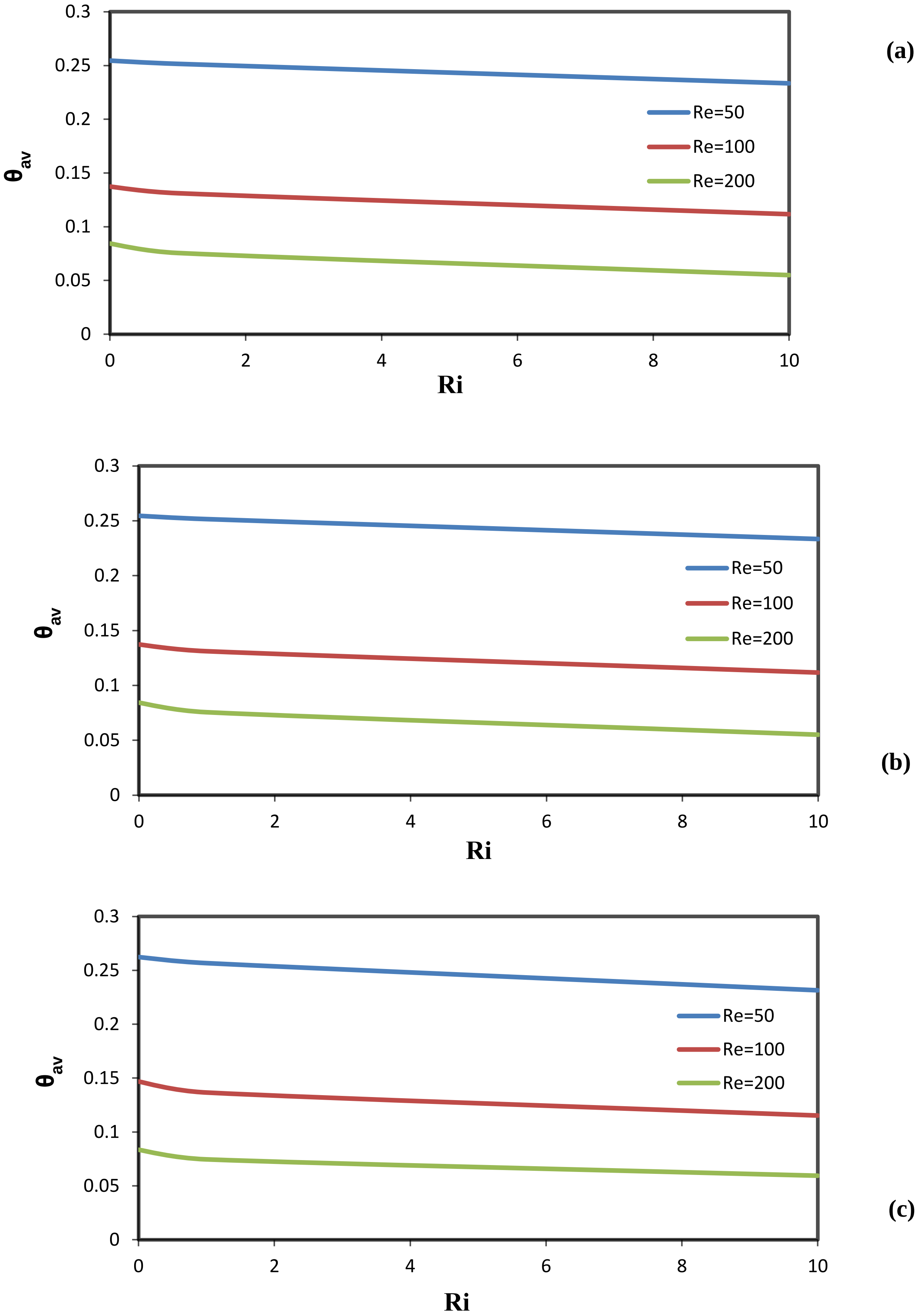

Fig. 9 Variation of mean bulk temperature with *Ri* for:
(a) H_{b2}=0.25L , (b) H_{b2}=0.5L , (c) H_{b2}=0.75L.